Geomechanics and Engineering, *Vol. 22, No. 6 (2020) 475-488*
DOI: https://doi.org/10.12989/gae.2020.22.6.475

Experimental and numerical investigation of expanded polystyrene (EPS) geofoam samples under monotonic loading

Omid Khalaj*[1], Seyed Mohammad Amin Ghotbi Siabil[2], Mehran Azizian[2], Seyed Naser Moghaddas Tafreshi[2], Bohuslav Mašek[3], Miloslav Kepka[1], Tomáš Kavalir[1], Michal Křížek[1] and Hana Jirková[1]

[1]*Regional Technological Institute, Univerzitni 8, 30100, Plzen, Czech Republic*
[2]*Department of Civil Engineering, K.N. Toosi University of Technology, Valiasr St., Mirdamad Cr., Tehran, Iran*
[3]*COMTES FHT, Průmyslová 995, 334 41, Dobřany, Czech Republic*

(Received February 3, 2020, Revised July 27, 2020, Accepted August 7, 2020)

Abstract. The recent increase in the use of Expanded Polystyrene (EPS) geofoam in construction and geotechnical projects has driven researchers to investigate its behavior, more deeply. In this paper, a series of experimental tests to investigate the stress-strain behavior and the mechanical properties of EPS blocks, under monotonic axial loading are presented. Four different densities of cylindrically shaped EPS with different dimensions are used to investigate the effects of loading rate, height and diameter, as well as the influence of the density of EPS on the stress-strain response. The results show that increasing the height of the EPS samples leads to instability of the sample and consequent lower resistance to the applied pressure. Large EPS samples show higher Young's modulus and compressive resistance due to some boundary effects. An increase in the rate of loading can increase the elastic moduli and compressive resistance of the EPS geofoam samples, which also varies depending on the density of the samples. It was also determined that the elastic modulus of EPS increases with increasing EPS density. By implementing an efficient numerical procedure, the stress-strain response of EPS geofoam samples can be reproduced with great accuracy. The numerical analysis based on the proposed method can used to evaluate the effect of different factors on the behavior of EPS geofoam.

Keywords: expanded polystyrene (EPS); geofoam; sample size; sample slenderness; strain rate; monotonic loading

1. Introduction

Expanded Polystyrene (EPS) geofoam is a type of cellular polymeric material with a history of successful applications in construction and geotechnical engineering. It is used in different applications where it is exposed to various kinds of stresses (Ossa and Romo 2010, Ngo *et al.* 2019). In the 1960s, Norway started to use the lightweight-fill function of EPS to develop road embankments over soft soils. Since then, other characteristics of EPS have made it a solution for a variety of construction problems which require light weight material capable of reducing vertical and lateral stresses with acceptable compression strength. This meant a rapid increase in the use of EPS in geotechnical projects such as embankment construction (Magnan and Serratrice 1989, Duskov 1991, Frydenlund and Aaboe 1994, Van Dorp 1996, Zou *et al.* 2000, Negussey *et al.* 2001, Newman *et al.* 2009, Khalaj *et al.* 2018, Ghotbi Siabil *et al.* 2019, Selvakumar and Soundara 2019, Gezgin and Cinicioglu 2019, Ghotbi Siabil *et al.* 2020), slope stability (Jutkofsky *et al.* 2000, Sheeley 2000, Srirajan 2001, Kim *et al.* 2019, Tavakoli *et al.* 2016), retaining structures (Negussey and Sun 1996, Elragi 2000, Jamshidi Chenari *et al.* 2018), bridge abutments (Williams 1990, Skuggedal and Aaboe 1991, McDonald and Brown 1993, Abu-Hejleh *et al.* 2003), buried pipes and culvert (Bartlett *et al.* 2015, Moghaddas Tafreshi *et al.* 2020, Azizian *et al.* 2020, Khalaj *et al.* 2020, Moghaddas Tafreshi *et al.* 2020). The high compressibility specification of EPS makes it an ideal material for reducing vertical and horizontal stress within the structure it is used. The basic concepts of the compressible inclusion function of EPS under static loading were investigated by Horvath (1997). Continuing investigation on this role of EPS has shown that the compressive strength of EPS geofoam depends on material density, strain rate and the confining stress/situation (Gao *et al.* 2011, Chen *et al.* 2019). The mechanical properties determine the capability of EPS slabs under compressive stress which leads to their deformation and disruption (Kwon *et al.* 2019). Strain rate is also an important factor which influences the bearing capacity of EPS, so it should be estimated as one of the working conditions parameters.

Although these studies cover a wide range of EPS geofoam characteristics, a decisive understanding of the EPS geofoam behavior is still demanding. Mohajerani *et al.* (2017) reported that a pervasive usage of EPS geofoam is still limited and further studies are necessary to develop standards in this area. One of the main shortcomings is the lack of information for EPS geofoam under static loading condition. This type of loading is present in the case of civil engineering structures, including retaining walls and road

*Corresponding author, Ph.D.
E-mail: khalaj@rti.zcu.cz

ISSN: 2005-307X (Print), 2092-6219 (Online)

Table 1 Material properties (ASTM D 6817/6817M-17)

Properties	EPS 15	EPS 19	EPS 22	EPS 29
Density (kg/m^3)	14.4	18.4	21.6	28.8
Initial elastic modulus, E_i (MPa)	2.5	4	5	7.5
Compressive resistance @1% axial strain (kPa)	25	40	50	75
Compressive resistance @5% axial strain (kPa)	55	90	115	170
Compressive resistance @10% axial strain (kPa)	70	110	135	200

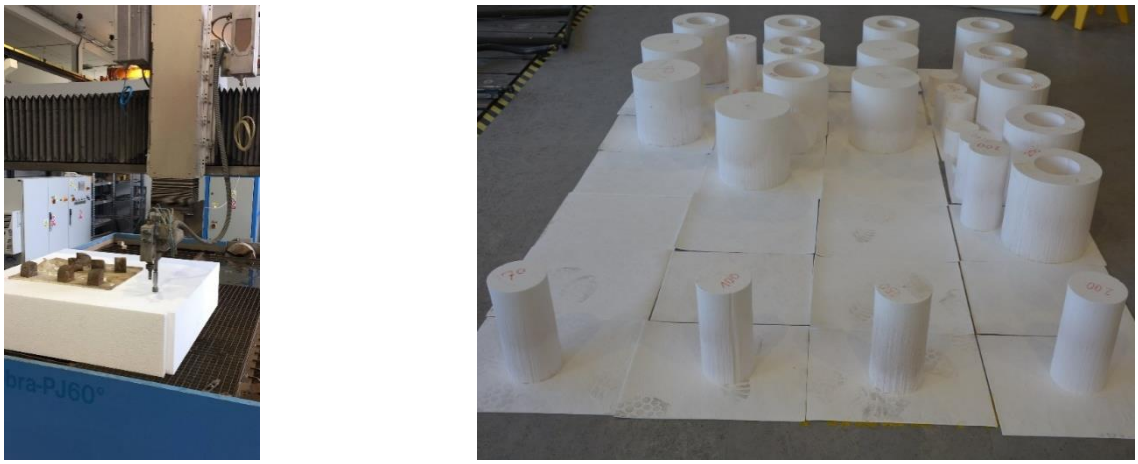

(a) (b)

Fig. 1 EPS samples preparation: (a) Water jet for cutting the samples and (b) Different sizes of samples cut by water jet

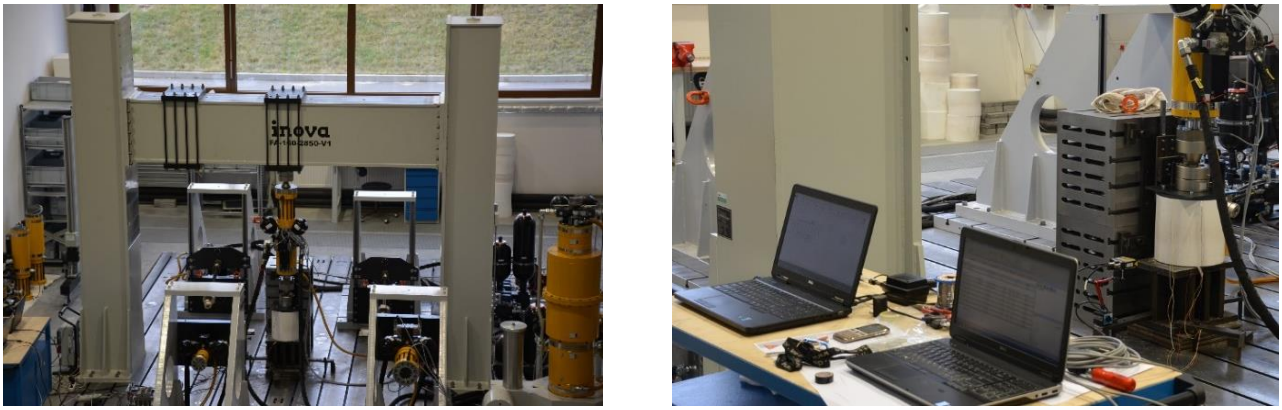

(a) (b)

Fig. 2 Preparation of test setup: (a) Testing equipment and (b) Sample setup

embankments where EPS geofoam is used as light backfill to reduce forces applied on foundations or structures. This study is intended to provide an understanding of the mechanical behavior of Expandable Polystyrene (EPS) subjected to monotonic compression loading with different strain rates. A series of uniaxial tests were carried out on cylindrical EPS geofoam specimens with different ratios of height (H) to diameter (D), different diameters (D) and different densities varying from 14.4 kg/m^3 to 28.8 kg/m^3. All the samples were cut from the middle part in order to place the pressure cells to monitor the pressure distribution within the EPS block.

Some researchers (Findley and Khosa 1956, Preber *et al.* 1994, Findley *et al.* 1989, Horvath 1998, Hazarika and Okuzono 2004, Chun *et al.* 2004, Hazarika 2006, Wong and Leo 2006, Meguid and Hossein 2017, Dehghanbanadaki *et al.* 2020) investigated the behavior of EPS geofoam blocks by numerical analyses. Chun *et al.* (2004) introduced a hyperbolic model in which the role of principle stress, principle strain, confining stress and the density of EPS block are considered. In this study, a robust numerical procedure based on Meguid and Hossein (2017), was also used to improve the understanding regarding the effect of EPS geofoam density, sample size and height to width ratio of the samples. This elastic isotropic model that is capable to involve the hardening response of EPS blocks' behavior, which is essential to obtain accurate results from numerical analyses of EPS blocks.

2. Experimental procedure

2.1 Material preparation

EPS is generally produced using two main processes, pre-expansion, and molding. The pre-expansion process heats polystyrene beads in a container at a temperature between 80ºC and 110ºC. During this stage, the original polystyrene beads expand into spheres commonly referred to as "pre-puff", which are approximately 50 times larger than the original polystyrene beads. Pre-puff is cooled to be stabilized for the next step which usually takes several hours. Afterwards, the cooled pre-puff is placed into a mold which is heated by steam to make it softer and more expandable. By the end of this stage, EPS blocks are left for several days to allow the outgassing of the blowing agent used in the manufacture, and to allow completion of the swelling and dimensional changes that are associated with the cooling process, which is called "seasoning". The EPS blocks used in this study were produced by the company IZOPOL Dvořák, S.R.O. (a local manufacturer in the Czech Republic) with 4 different densities. The compressive strength of the samples were measured using according ASTM D 6817 (see Table 1). Elastic modulus derived from the figures of experimental analyses at 1% strain values, and the Poisson's ratio values considered as 0.1 based on Duskov *et al.* (1998) suggestion. EPS samples were prepared by cutting larger blocks into cylinders using a water-jet (Fig. 1a). The dimensions of the samples were chosen to investigate the effect of the ratio of diameter to height (H/D) within different diameters (D) of samples (Fig. 1b).

2.2 Testing equipment

A universal hydraulic loading system equipped with high speed precise data acquisition was used to apply the uniaxial vertical loading. The loading frame which supports the hydraulic cylinder weighs 4.5 tons with a capacity of 32 tons. A hydraulic jack with nominal span and load of 250 mm and 100 kN was used to apply the loading force to the upper and bottom surface of EPS sample through rigid smooth steel plates and limited from horizontal movements. The applied load was measured by an inline load transducer with a capacity and accuracy of 100 kN and 0.02% which was double checked by an oil pressure sensor inside the hydraulic cylinder. The vertical movement of the hydraulic cylinder is controlled by an internal displacement transducer which can control the movement of the hydraulic piston with an accuracy of 0.01%. The transferred pressure to EPS blocks was measured using four pressure cells; two of them were installed in the middle of the block and the other two on the top of the EPS sample. The pressure cells were made of a thin layer of polyester with a sensing area of 25.4 mm capable of measuring a maximum pressure of 700 kg/cm^2 with an accuracy of 0.01%. The whole system is controlled by the central data acquisition system with a sampling rate of 25 Hz - which covers the precise measurement for static tests. Fig. 2(a) and 2(b) show the real view of the testing system.

2.3 Testing program

Table 2 Parameters of test program

Test Group	No. of tests	Sample Diameter (D)	Sample Height (H)	H/D ratio	EPS density	Strain rate	Purpose of tests
		mm	mm		kg/m^3	s^{-1}	
A	24	150	150, 300	1, 2	14.4, 18.4, 21.6, 28.8	0.001, 0.01, 0.1	Preliminary tests to check the sensors, system, and tests reproducibility and repeatability
B	4	150	150, 180, 240, 300	1, 1.2, 1.6, 2	28.8	0.001	Effect of sample height to diameter (H/D)
C	9	300	300	1	14.4, 18.4, 21.6	0.001, 0.01, 0.1	Effect of loading strain rate
D	2*	100, 200, 300	100, 200, 300	1	18.4	0.001	Effect of EPS sample diameter (D)
E	6*	150	150, 300	1, 2	14.4, 18.4, 21.6, 28.8	0.001	Effect of EPS sample density (γ)

*Test repetitions from previous test Series are not counted

The testing program was designed in a way that the most important parameters which affect the behavior of EPS could be investigated. The program is divided into five Test Series to check the effects of H/D (height to diameter of the sample), strain rate, Sample diameter (D) and EPS density (γ) on the stress-strain behavior and the side deformation of the EPS samples. Table 2 shows a summary of the testing program.

Tests in group A were carried out to check the tests' repeatability, performance of the loading system, loading frame, transducers, measuring and control system. All sizes and densities of samples were used to check the compatibility of the test system at different strain rates. The repeatability of the tests shows less than 2% difference, which confirms that the whole loading and measuring system works properly.

Tests in group B were carried out to investigate the effect of Height to Diameter ratio (H/D) of EPS samples with density of 28.8 kg/m^3. The diameter of the samples was 150 mm with various sample heights (150, 180, 240 and 300 mm) to achieve different H/D ratios equal to 1, 1.2, 1.6 and 2. The loading was applied with a constant strain rate of 0.001 s^{-1} to simulate a drained situation (static loading) which gives enough time for the internal air and water to leave the sample and achieve zero pore air and water pressure during the tests.

Tests in group C were carried out to investigate the effect of strain rate on the behavior of the stress-strain curves of EPS. The loading was applied with different strain rates of 0.001, 0.01 and 0.1 s^{-1} up to the maximum available span/load capacity of the hydraulic loading system. The sample height and diameter was 30 cm (H/D = 1) with various densities of EPS (14.4, 18.4, 21.6 kg/m^3). Tests in group D were carried out to investigate the effect of the

(a) (b)

Fig. 3 Measurement devices installed on EPS samples: (a) Different layers of EPS placed in the loading jack and (b) A pressure cell placed on top of the EPS sample

change in the diameter of the EPS samples. The diameters of the samples were 10, 20 and 30 cm for this test series. One of EPS density (18.4 kg/m^3) and H/D ratio equal to 1 were chosen. The constant strain rate of 0.001 s^{-1} to simulate the drained situation gives enough time for the internal air and water to leave the sample and make zero pore air and water pressure during the tests. In Test Series E, samples with densities of 14.4, 18.4, 21.6, 28.8 kg/m^3 were tested to identify the effect of EPS density. Sample diameter was 15 cm with H/D = 1, 2 and the strain rate was 0.001 s^{-1}. As well as all these measurements, the relaxation of all the samples after the tests was manually measured at different time intervals up to 6 months after the tests to investigate the short and long-term elastic and plastic deformation of the EPS samples.

3. Test results

3.1 Preliminary evaluations

Preliminary tests of Test Series A were carried out to check various components of the loading and measurement systems under different loading conditions. Each dimension and density of the EPS blocks in Table 2 was prepared from 6 layers of EPS geofoam blocks (Fig. 3(a)). Pressure cells were placed between the EPS blocks to find out if it was necessary to use more pressure cells in different layers of EPS geofoam (Fig. 3(b)). The results show that with an increasing number of EPS layers, the efficiency of the whole testing system is reduced. Due to a lack of lateral support for the EPS blocks, a buckling mode of failure appears with increasing load which leads to instability of the system. This phenomenon certainly affects the results and causes a different pressure distribution between adjacent blocks throughout the height of the arrangement of the EPS blocks. Besides this, the results show that the cubic shape of the EPS samples might induce varied stress distribution on the blocks, thus, the cylindrical sample shape was chosen for the rest of the tests.

3.2 Main test results

3.2.1 Effect of height to diameter ratio (H/D)

Test Series B was planned to investigate the effect of EPS sample height or H/D at a specific diameter (D) on the stress-strain behavior of the EPS blocks. The results from Test Series A had shown that increasing the number of EPS layers to increase its height with a constant diameter results in buckling and instability of the blocks. Thus, in this Test Series single EPS blocks with H/D of 1, 1.2, 1.6 and 2 were tested. The density of EPS was 28.8 kg/m^3 and the strain rate was 0.001 s^{-1}. Fig. 4 shows the stress-strain curve of EPS geofoam with H/D ratio of 2. Previous research (e.g., Stark *et al.* 2004) showed that a typical stress-strain curve of EPS geofoam under uniaxial compression loading consists of the following parts: (1) Initial linear behavior, (2) Yielding, (3) Linear-work hardening and (4) Nonlinear with work hardening response. A similar behavioral classification can be made on the stress-strain curve obtained from our tests, as shown in Fig. 4. However, zones 1 and 2 span a much smaller portion of the figure, and hence are not separated.

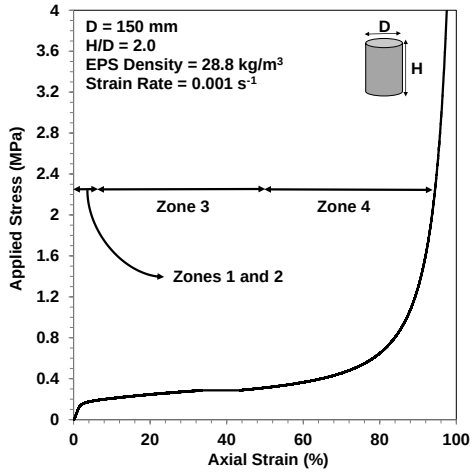

Fig. 4 Typical stress-strain curve for EPS samples

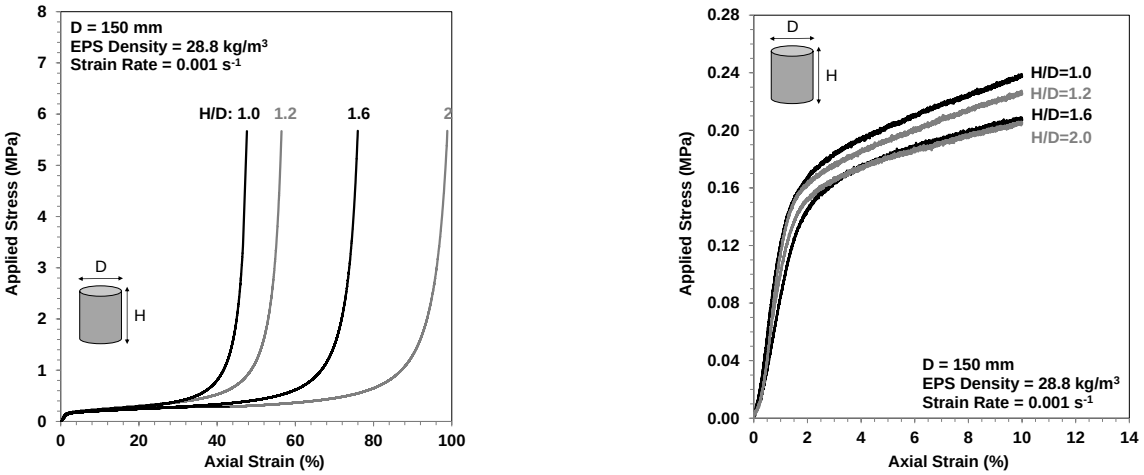

(a) (b)

Fig. 5 (a) Stress-strain curve for different H/D ratios up to maximum compression and (b) Stress-strain curve for different H/D ratio up to 10% strain

(a) (b)

Fig. 6 Deformation and failure mechanisms: (a) Regular sample deformation occurring for lower H/D and (b) Buckling-form deformation occurring at larger H/D

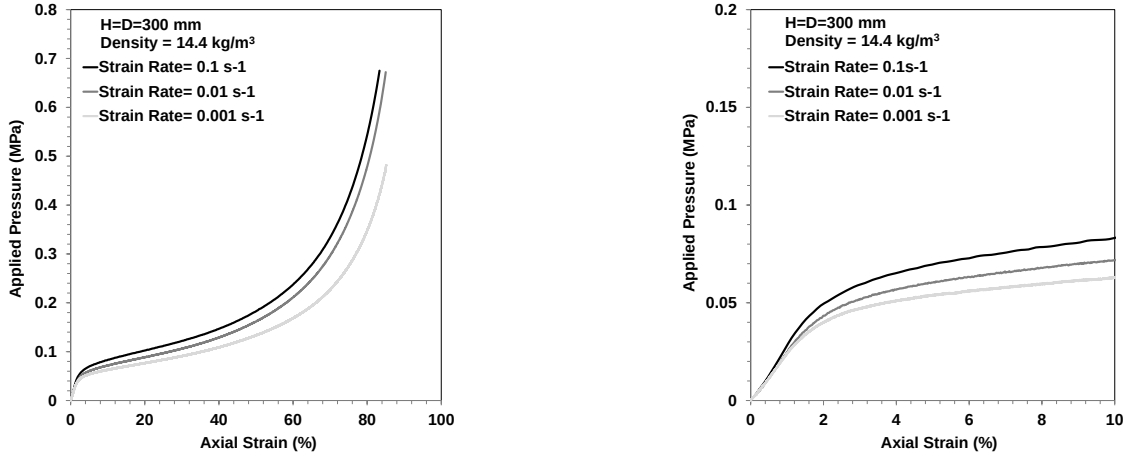

(a) (b)

Fig. 7 (a) Stress-strain curve at different strain rates on various densities of EPS samples with height and diameter of 300 mm and (b) The stress-strain curve up to 10% strain under similar condition

The practical point behind the geofoam EPS blocks are their protection against the high level of deformation, and this issue is so practical in geotechnical issues and projects. In this regard, some projects are implemented through EPS

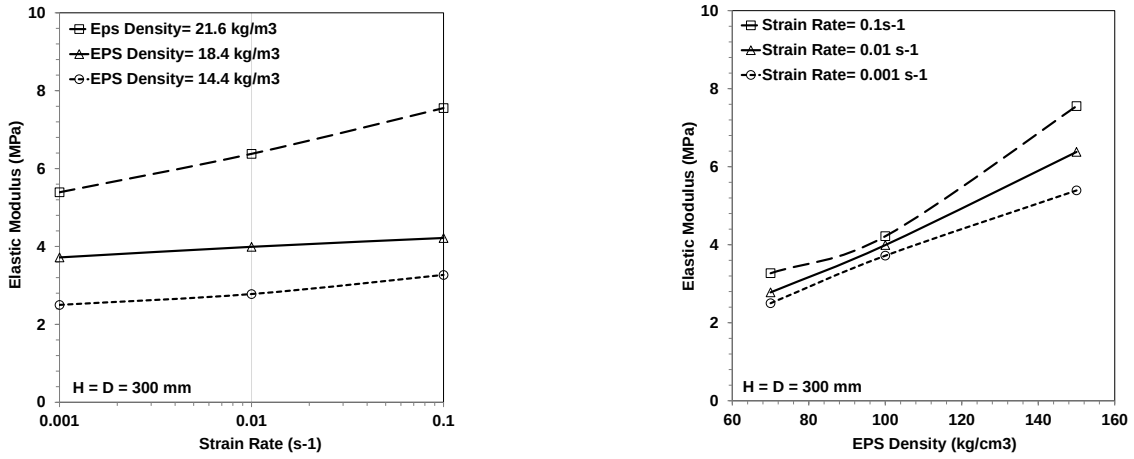

(a) (b)

Fig. 8 (a) Variation of EPS geofoam elastic modulus with strain rate for different densities of EPS and (b) Variation of EPS geofoam elastic modulus with EPS density at various strain rates

blocks in which dimensions having undeniable roles such as the column of bridges. In this approach, the dimensions have practical role by giving better response. For example, EPS block with H/D=2 has 80% axial strain without dominant increase in stress level, so it is so important in geotechnical perspectives to know the gamut of strain values under applied stresses. Fig. 5 shows the result of the uniaxial compression test with a strain rate of 0.001 s^{-1} on the EPS blocks with a density of 28.8 kg/m^3 and different H/D ratios. With increasing H/D ratio, the linear work-hardening zone (zone 3) significantly increases according to Fig. 5(a). Thus at a specific ultimate stress (say 5.5 MPa in this study), the final strain for H/D=1, 1.2, 1.6 and 2 is approximately 45%, 55%, 75% and 97%, respectively. As tests were performed under stress-controlled conditions, the taller samples (with larger H/D) buckle faster and thus the strains are much larger on reaching a specified magnitude of applied pressure.

Additionally, Fig. 5(b) demonstrates the stress-strain curves of the sample for up to 10% strain. It is evident that samples with smaller ratios of H/D sustain slightly larger compressive stress compared to taller specimens at this range of strains. The ultimate deformation of shorter and taller EPS samples depicted in Fig. 6 also suggests that the shorter samples have been compressed evenly along their vertical dimension while the taller samples have experienced bending (visible on the right side of the sample) due to premature buckling. Therefore, taller EPS samples are more likely to demonstrate buckling type failure mechanisms and reduced compressive strength.

3.2.2 Effect of strain rate

In Test Series C, three strain rates of 0.1, 0.01 and 0.001 s^1 were selected to evaluate the effect of loading speed. The samples' height and diameter were 300 mm and the EPS densities were 14.4, 18.4, 21.6 kg/m^3. Previous observations by Trandafir *et al.* (2010) showed that the behavior of EPS geofoam is greatly dependent on the rate of loading. According to Fig. 7(a), EPS geofoam exhibits larger compressive strength with increasing strain rate and the difference in the compressive strength between the selected rates increases with increasing strain amplitude. It can be understood that, as the strain rate increases, the increment of increase in the compressive strength of EPS samples gradually decreases. When the rate of applied pressure is slow, EPS bubbles have enough time to deform and eventually destruct under pressure. As the loading rate increases, the bubbles are forced to contract evenly under the confinement and a smaller number of them might become damaged (comparable to what happens to saturated soil during consolidation). Thus when pressure is applied in a gentle manner, more EPS bubbles are destroyed and therefore a lower compressive strength is observed. The described mechanism seems to be more valid for lower density EPS geofoam, as the bubbles are larger. The structure of denser EPS geofoam consists of less air and thus might be less sensitive to the loading rate, but this requires further investigation. Fig. 7(b) shows the stress-strain response up to 10% strain under the same condition. It is evident that the above discussion is also applicable up to these strain levels.

Fig. 8(a) and 8(b) display the variation of Young's modulus for different densities of EPS geofoam with the strain rate. Obviously, the higher density EPS shows a larger elastic modulus, and the elastic modulus increases as the strain rate increases. Contrary to the observations made on the whole stress-strain plots, the influence of the strain rate on the Young's modulus of the EPS samples increases with increasing EPS density. This might be because the elastic moduli are obtained from the elastic region of the plots, which are not affected by the bubbles interaction phenomena on the overall plots (Fig. 7). When the EPS material is elastic (1% strain), the governing influential factor depends on the EPS material itself. It can be concluded that when EPS geofoam is expected to work under elastic conditions, the Young's moduli of the higher density EPS is more dependent on the strain rate, while beyond the elastic limit, lower density EPS would be more sensitive to the loading rate.

3.2.3 Effect of sample size

In this Test Series, the effect of sample size on the stress-strain response of EPS geofoam is investigated. EPS

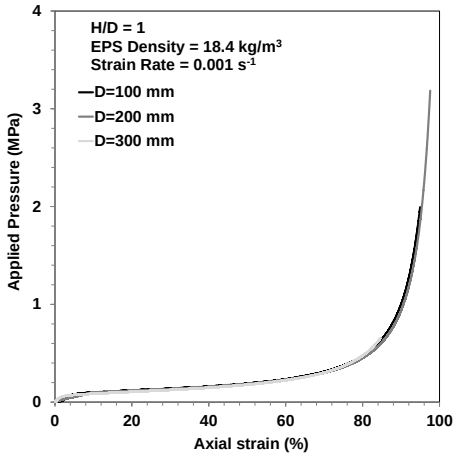

Fig. 9 Overall stress-Strain curve for different sizes of EPS samples with H/D = 1, density of 18.4 kg/m^3 and loading rate of 0.001 s^{-1}

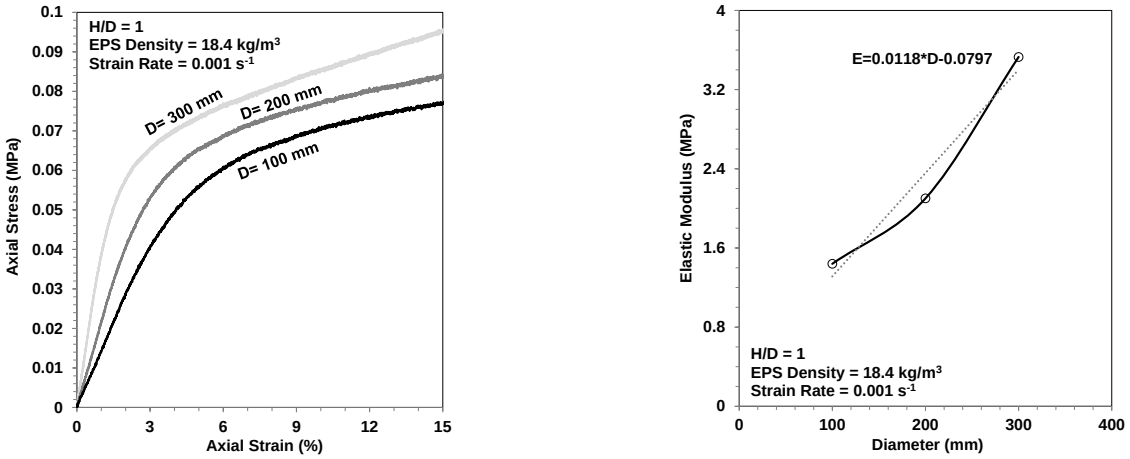

(a) (b)

Fig. 10 (a) Stress-strain curve for different sizes of EPS samples for up to 15% strain and (b) Variation of elastic modulus with sample diameter, all with loading rate of 0.001 s^{-1}, EPS density of 18.4 kg/m^3 and H/D = 1

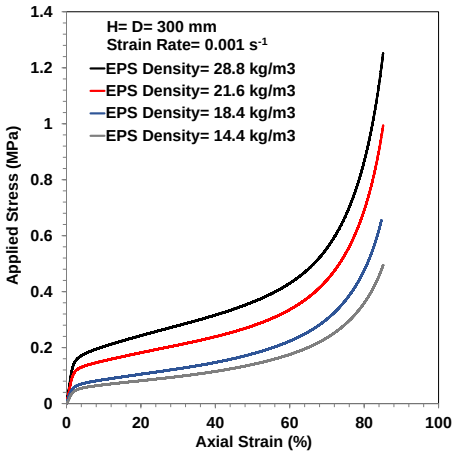

Fig. 11 Stress-Strain curve for different EPS densities at H=D=300 mm and strain rate of 0.001 s^{-1}

samples with diameters 100, 200 and 300 mm (representing small, medium and large size) with H/D ratio of 1 were selected and loaded at a rate of 0.001 s^{-1}. From Fig. 9, it can be seen that the overall stress-strain response of EPS geofoam samples with varying size does not have a significant difference and all the samples behave in similar ways. However, this observation seems to be invalid if certain parts of the stress-strain plots are compared.

The initial part of the stress-strain curve in Fig. 9 (up to 10% strain) was extracted and displayed in Fig. 10a to evaluate how these curves differ at the most important strain range (e.g., ranges of elastic modulus and compressive strength). It is evident that the compressive resistance of the larger samples increases with a larger slope, and such samples have shown greater resistance, thus the Young's moduli of larger samples are greater than the smaller samples. Newman *et al.* (2009) also discovered that the elastic modulus of the EPS geofoam sample increases as the sample size increases, thus the moduli of EPS used in the numerical analyses could be selected up to a few times higher than the moduli obtained from testing the small samples. Fig. 10(b(shows the variation of elastic moduli vs. the diameter of EPS samples. Using a linear equation (Fig. 10(b)), the dependency of elastic modulus on the sample diameter can be expressed as:

$$E = 0.0118D - 0.0797 \quad (1)$$

where E stands for elastic modulus (MPa) and D is the

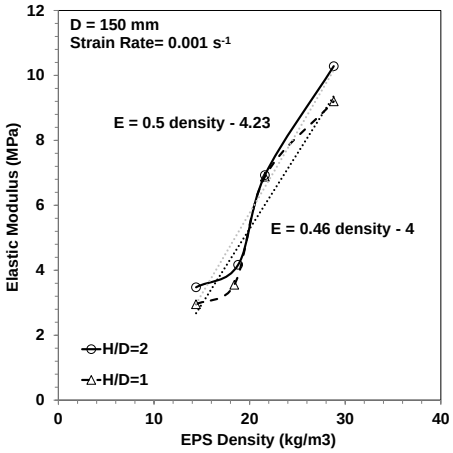

Fig. 12 Variation of Young's modulus vs. EPS density for samples with H/D=1, 2 and strain rate of 0.001 s^{-1}

sample diameter (mm). It should be noted that this equation is derived for EPS 19 at a loading rate of 0.001 s^{-1} and can be used to estimate the elastic modulus for the range of diameters used in this study (i.e., 100-300 mm). Although some research have investigated the effect of sample size (Elragi *et al.* 2001), no such relation is developed yet. Negussey and Anasthas (2001) have reported that increasing sample size from 50 to 600 mm can increase Young's modulus by 112%. However in this study, increasing sample size from 100 to 300 mm caused about 220% increase in Young's modulus. Therefore, a final generalization on this issue needs further studies.

3.2.4 Effect of EPS density

In Test Series E, the effect of EPS density on the stress-strain behavior and the Young's modulus of EPS samples is investigated. For these tests, the height and diameter of the EPS samples was 300 mm and the rate of loading was 0.001 s^{-1}. Fig. 11 shows the overall stress-strain curves for various densities of EPS geofoam. As expected, the compressive resistance of EPS geofoam increases with increasing EPS density. EPS with densities 14.4 and 18.4 kg/m^3 are very close in terms of mechanical properties, thus their stress-strain plots move adjacent to each other over a large of portion of strains. The plots of different densities vary at an almost constant difference from 50% strain up to the end of loading. The final compressive pressure (at about 90% strain) sustained by EPS with densities 14.4, 18.4, 21.6 and 28.8 kg/m^3 are approximately 0.5, 0.65, 0.95 and 1.3 MPa, respectively.

Fig. 12 shows the variation of Young's moduli for the tested EPS densities and a possible linear fit for the H/D=1 and H/D=2 cases. It should be noted that the Young's modulus for 14.4 kg/m^3 EPS density is slightly larger than the estimated value calculated from the equation obtained from larger densities (the equations are shown on the plots for the relevant trend line). However, the upper and lower boundary equations (H/D=2 and H/D=1, respectively) for estimating the elastic moduli based on the EPS density can be expressed as:

$$E=0.5\rho-4.32 \quad (2)$$

$$E=0.46\rho-4 \quad (3)$$

in which ρ (kg/m^3) and E (MPa) stand for EPS density and elastic modulus, respectively.

4. Numerical analysis

To provide further understanding on EPS geofoam behavior, numerical modelling was carried out and presented in this section. There are several numerical (and of course numerically implemented analytical methods) for addressing the behavior of EPS geofoam material (Findley and Khosa 1956, Preber *et al.* 1994, Findley *et al.* 1989, Horvath 1998, Hazarika and Okuzono 2004, Chun *et al.* 2004, Hazarika 2006, Wong and Leo 2006, Meguid and Hossein 2017, Dehghanbanadaki *et al.* 2020). Hazarika (2006) introduced a constitutive model for EPS geofoam under large-strain and rapid loading. The model encompasses the size and shape factors and the density of EPS geofoam. The yield function is defined by taking EPS as a von Mises type material, and considering the isotropic hardening approach. Wong and Leo (2006) established a simple elastic-plastic hardening constitutive model using a series of triaxial tests on EPS samples with the confining pressures ranging from 0 to 60 kPa. The model includes six rheological constant parameters depending on the isotropic elastic behavior, the first yield stress, the hardening rate, the flow rule and the dilatancy behavior. Neither the time dependency (creep) nor the size and shape factors of the EPS specimens are not addressed in this constitutive model.

A common method is LCPC (Laboratoire Central Ponts et Chaussees) (Magnan and Serratrice 1989), which is simplified form of the Findley approach (Findley *et al.* 1989) as:

$$\epsilon_t=\left(\frac{\sigma}{Eti}\right)+at^n \quad (4)$$

$$a= 0.00209\left(\frac{\sigma}{\sigma y}\right)^{2.47} \quad (5)$$

$$n= -0.9\times Log_{10}\left[1-\left(\frac{\sigma}{\sigma y}\right)\right] \quad (6)$$

$$\sigma_y= 6.41\gamma-35.2 \quad (7)$$

$$E_{ti}= 479\gamma-2875 \quad (8)$$

In this equation E_{ti} (kPa), γ (kg/m^3) and σ_y (kPa) are initial tangent Young's modulus, density and yield strength of EPS geofoam, respectively. In this model, the strain values are directly related to the imposed stress and the density of EPS geofoam (Chun *et al.*, 2004). Effect of loading time on the behavior of EPS geofoam is considered in the LCPC model. Chun *et al.* (2004) introduced a hyperbolic model in which the behavior of EPS material is based on the principle stress, principle strain, confining stress and the density of EPS block. This model is represented as follows:

$$\sigma_1= a{\epsilon_1}^b{}_{(\%)}/\ (c+ {\epsilon_1}^b{}_{(\%)}) \quad (9)$$

$$a= -60.955+9.843\gamma+0.339\sigma_3 \quad (10)$$

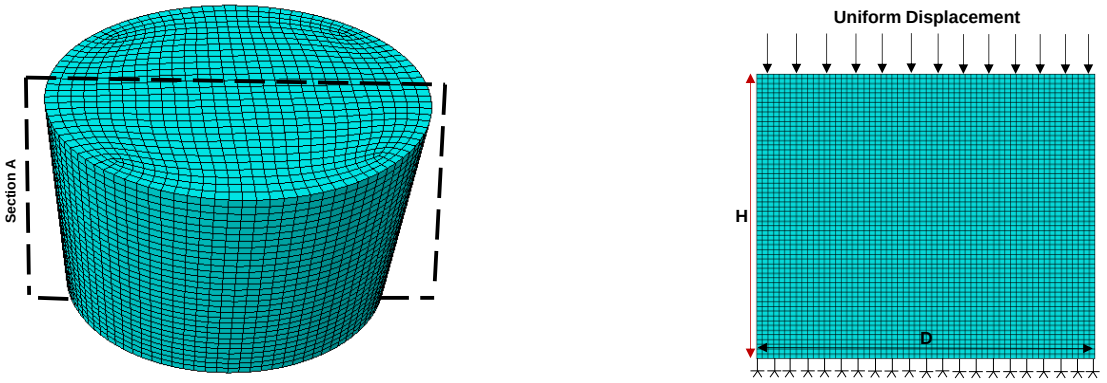

(a) (b)

Fig. 13 (a) Full 3D mesh of the samples EPS geofoam in ABAQUS and (b) Typical 2D side view with boundary conditions

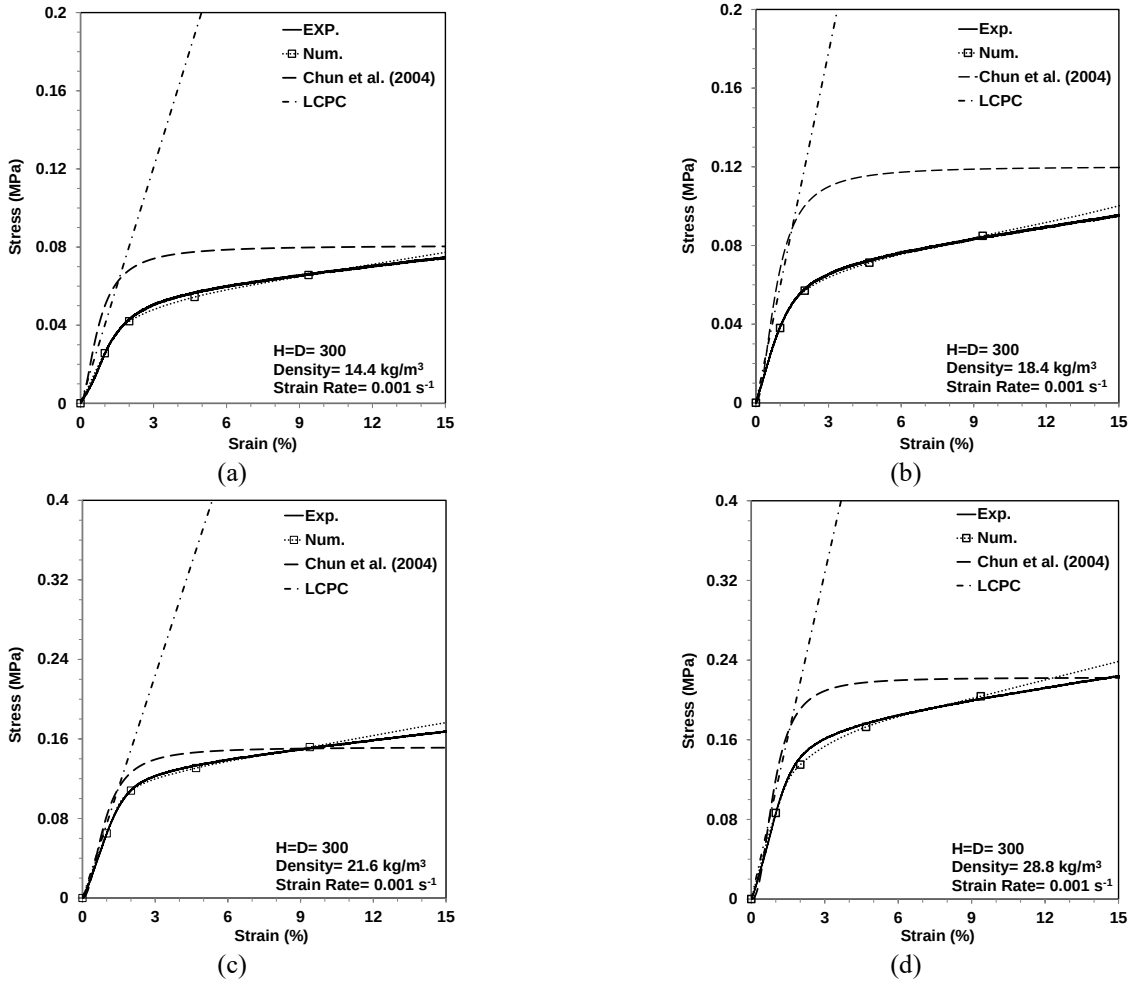

(a) (b) (c) (d)

Fig. 14 Comparison of stress-strain response for EPS densities of (a) 14.4 kg/m^3, (b) 18.4 kg/m^3, (c) 21.6 kg/m^3 and (d) 28.8 kg/m^3 using various numerical methods

$$b= 1.135+0.042\gamma-0.008\sigma_3 \quad (11)$$

$$c= -0.437+(0.102\gamma)-(0.002\gamma^2)+(0.011\sigma_3)-(0.00039\gamma\sigma_3) \quad (12)$$

In this equation, ϵ_1 (%), σ_3 (kPa) and γ (kg/m^3) are the major principle strain, confining stress, and the value of the density, respectively. The important point of this hyperbolic model is that the strain-dependent tangent modulus E_t (kPa) is a function of confining stress, density, and strain:

$$E_t= d\sigma/(d\epsilon_{1\,(\%)}/100) \quad (13)$$

$$E_t= [abc{\epsilon_1}^{b-1}{}_{(\%)}/({\epsilon_1}^{2b}{}_{(\%)}+2c\,{\epsilon_1}^{b}{}_{(\%)}+c^2)]*100 \quad (14)$$

The key point in this constitutive model is that it was derived from straining (at rate of 1 mm/min) of cylindrical EPS geofoam samples with diameter and height of 50 and 100 mm, respectively.

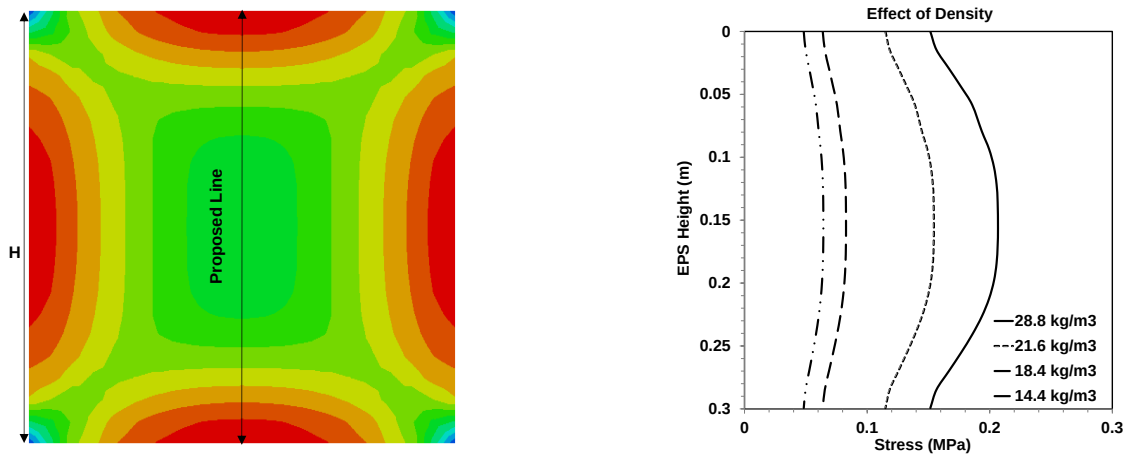

(a) (b)

Fig. 15 (a) Typical stress contour at sample symmetry plane for EPS block under the 5% percent axial strain and (b) stress along the centre line of different densities of EPS geofoam under The 5% axial strain

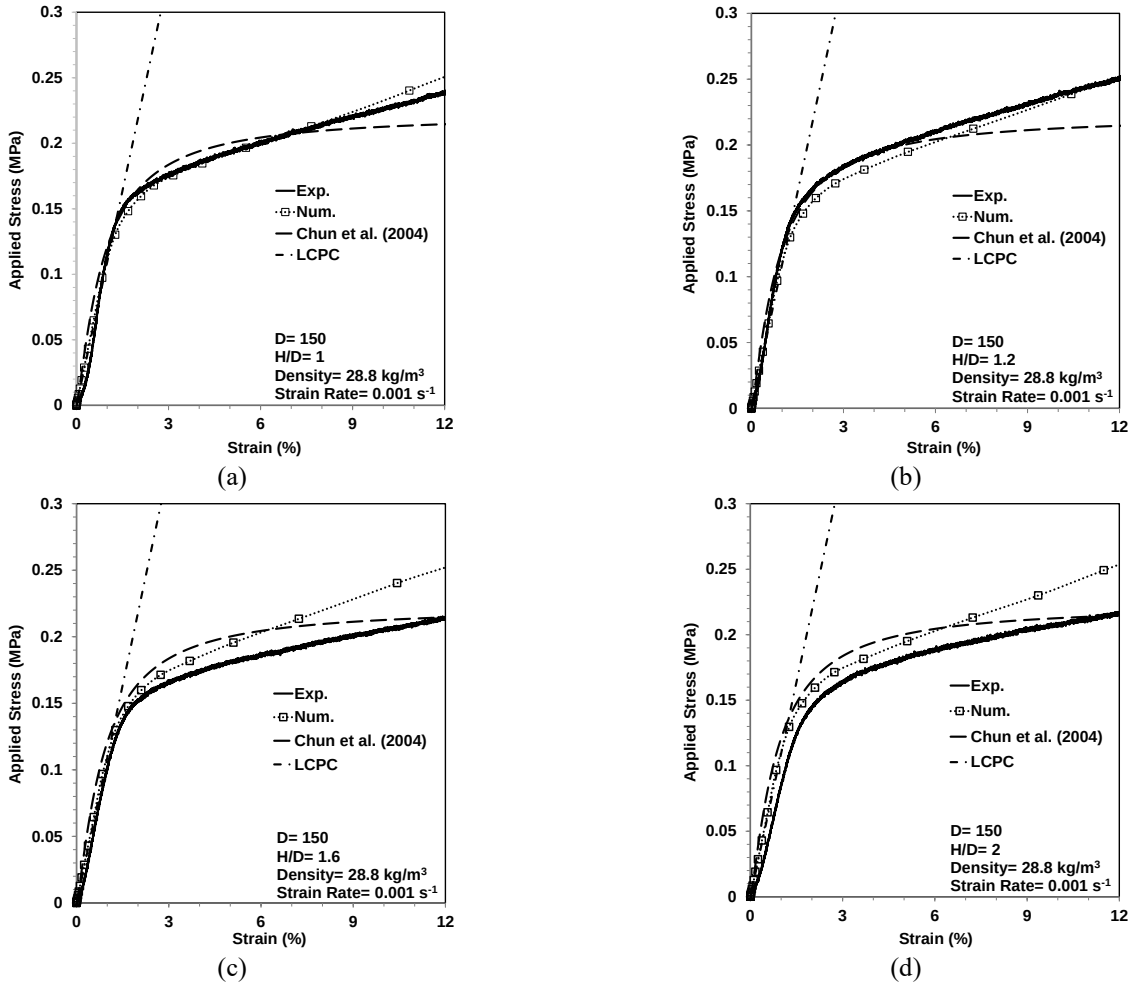

(a) (b) (c) (d)

Fig. 16 Stress-strain response of 28.8 kg/m^3 EPS geofoam samples using various numerical methods for (a) H/D=1, (b) H/D=1.2, (c) H/D=1.6 and (d) H/D=2

Meguid and Hossein (2017) suggested a robust modelling procedure for numerical simulation of EPS geofoam behavior. In this model, the elastic isotropic model, Misses yield criteria and associated flow rule were considered to define the elasticity and plasticity of EPS geofoam, respectively. This method is capable of capturing the hardening of EPS material as a key factor in the response of EPS geofoam blocks. To define the plasticity, the nominal values of strain and stress should be converted to their real values. Owing to this fact, Eqs. (15)-(18) have

been proposed for converting experimental results to numerical input values in the current study:

$$\epsilon_{true} = Ln\ (1+\epsilon_{nominal}) \quad (15)$$

$$\sigma_{true} = \sigma_{nominal} / (1-\nu\ \epsilon_{nomimal})^2 \quad (16)$$

$$\epsilon_{true} = \epsilon_{elastic} + \epsilon_{plastic} \quad (17)$$

$$\epsilon_{elastic} = \sigma_{true} / E \quad (18)$$

Although some might use the Mohr-Coulomb model for EPS geofoam, The pivotal point in EPS blocks' response is the hardening after the 1% strain (elastic gamut). In some analyses the maximum deformations are in the threshold of elastic area, so it is viable to be mentioned that the Mohr-Coulomb is practical in the little deformation values. On the other hand, the employed model in numerical analyses is capable to see the hardening occurring over the elastic threshold (see Fig. 14).

4.1 Modelling the uniaxial tests

In order to have a better knowledge of EPS geofoam blocks, the mentioned procedure in the above (Meguid and Hossein 2017) was implemented in 3D finite element numerical models using ABAQUS (Simulia 2013). The model dimensions and loading patterns are similar to those of test samples. Fig. 13(a) shows full 3D mesh of modelled sample with eight-node linear brick elements (C3D8) and Fig. 13(b) shows a typical 2D side view of the models with the proposed loading. To simulate the uniaxial compressive tests, the base of EPS models was fixed and compressive loads were applied at the top of models. In all numerical analyses, the EPS blocks' tips were banned from horizontal directions, in which the symmetric response is clear (see Fig. 15(a)).

4.2 Numerical results

Results of the numerical simulation for various factors are presented in this section. Fig. 14 show the stress strain curve for different EPS densities using the implemented methods compared to the tests. For these cases, the height and width of EPS geofoam sample is 300 mm and the strain rate is 0.001 s^{-1}. It is clear that the numerical method produces the best match with test results for all of the cases. Although Chun *et al.* (2004) method produces an overall reasonable trend for the whole range of strains, the values are not close to the experimental results at a great part of the stress-strain curve. Using this method, the stress strain curve for EPS with density of 21.6 kg/m^3 shows the best match with test results. On the other hand, using LCPC method, the results are only valid up to strain level of 1% and beyond this point, the stress increases linearly with strain and no specific yielding point exist. Therefore, LCPC is not a reliable method for the strain values beyond 1%. The Chun method is appropriate for an initial evaluation and provides best results for intermediate EPS densities (i.e., 21.6 kg/m^3). The most reliable method for predicting stress-strain behavior of EPS is the numerical method by Meguid *et al.* (2017), also incorporated in this study.

The stress contour within the symmetric plane of EPS sample is presented in Fig. 15(a). It is clear that the stress is maximum in the middle (core) of the sample and at the outer top and bottom edges. The main portion of applied pressure is sustained by an internal core, extended diagonally to the upper and bottom of EPS sample. Thus with this stress gradient at the two ends of the sample, and stress concentration at the external edges, the cracking of EPS sample edges under loading plate is explicable. Fig. 15b shows stress amplitude along the central core of EPS geofoam sample height. With increase in density of EPS geofoam, the EPS strength increases and the stress amplitude at a specific height increases with increase in EPS density. Furthermore, it shows that the stress values are maximum at the center of the samples and it decrease gradually moving from the center toward the bottom and upper surface.

Fig. 16 shows the effect of height to diameter ratio of EPS samples using different numerical methods compared to the test results. For all of H/D cases in the numerical analysis, the stress-strain response of H/D=1 was used. It is clear that the adopted numerical procedure yields the best fit for the experimental data for H/D=1 and H/D=1.2. For the larger H/D ratios, the numerical method somehow overestimates the applied pressure for a certain stress. This might be due to the fact that the numerical model is much more idealistic in terms of material quality and its distribution over the whole volume of the sample. In reality, the samples are not completely intact and they certainly include points of weakness such as micro-cracks. Furthermore, the EPS material is not evenly distributed within the sample volume, causing a varying stiffness in the sample. For these reasons, taller samples are more likely to buckle under compression. However, such fact is neglected in the numerical samples due to inherent idealization of such FEM modelling. Finally, although the overall trend is acceptable for all H/D cases using test data for H/D=1, it is best to use the stress-strain values of the specific H/D under study. Similar to previous results, it can be seen that Chun model also provides reasonable estimation for the whole strain range, while LCPC is only valid up to about 1% strain.

Fig. 17(a) presents the typical contour of lateral deformation (in z or x direction) of EPS geofoam samples. As seen, the deformations at the side region of the samples is negligible. This phenomenon is due to the very low Poisson's ration of EPS geofoam (Stark *et al.* 2004). Poisson's ratio of EPS geofoam is relatively small and close to zero. Normally, this slight Poisson's ratio value can be assumed zero, however it would be slightly larger than zero before yielding strain (i.e., 10%) and can become slightly negative when EPS geofoam is compressed sufficiently. The negative Poisson's ratio at this condition is the result of destruction of air bubbles and the inward collapse of the EPS structure.

For clarification, the sample diameter under loading (initial sample diameter plus the lateral deformation) vs. the value of deformation in one side is shown in Fig. 17(b). Due to very low Poisson's ratio, the difference between lateral deformation plots of different H/D ratios is insignificant.

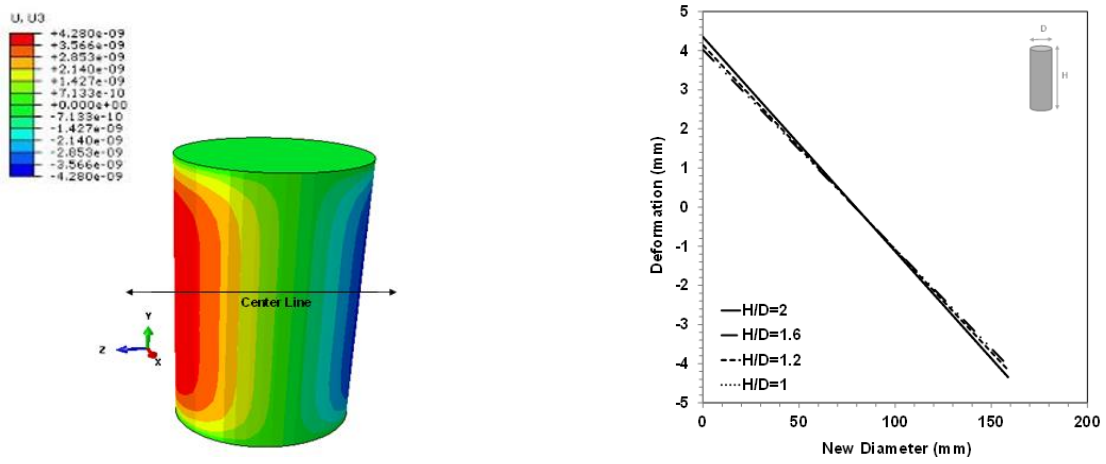

(a) (b)

Fig. 17 (a) Typical contour of lateral strain of EPS geofoam samples along z-axis under compressive loading and (b) Lateral deformation of EPS geofoam samples with different H/D ratios under the strain level of 10%

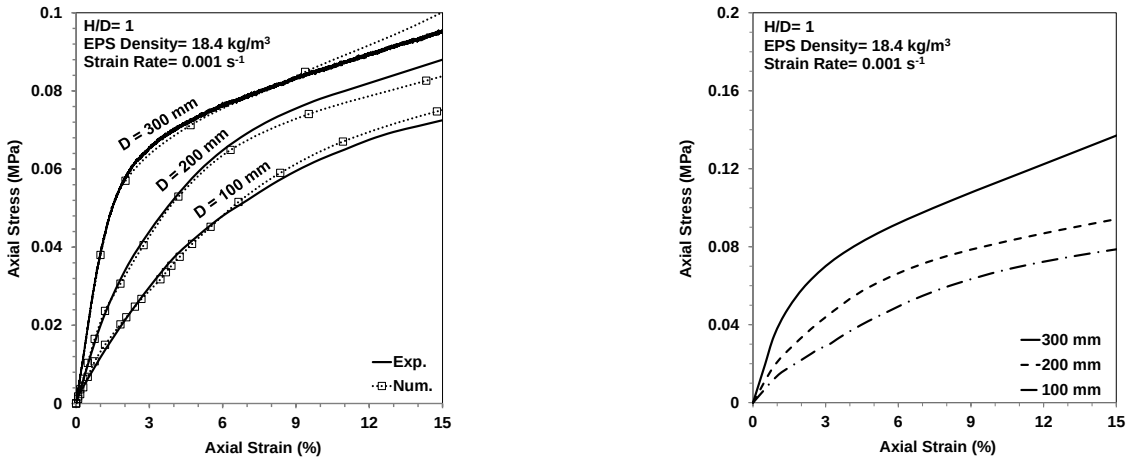

(a) (b)

Fig. 18 (a) Comparison of experimental and numerical methods on the effect of EPS sample size and (b) Stress at the centre of EPS geofoam sample vs. axial strain for different sample dimensions

Fig. 18(a) shows the effect of samples' size with numerical and experimental results. The numerical results are in good agreement with the experiments. In Fig. 18(b), the stress values at the center of the samples vs. axial strain is plotted for various sample sizes. With an increase in the sample size, the stress required to generate a specific strain in the samples is increased for larger samples. At 15% axial strain, samples with D= 300 and 200 mm sustain 47% and 21% greater pressure compared to samples with D= 200 mm and 100 mm, respectively. As noted before, large samples show larger strength due to the size effect of EPS geofoam.

5. Conclusions

A series of tests was performed on EPS geofoam samples to assess the effect of sample size, sample density, strain rate and sample height (H/D ratio) on the stress-strain response and elastic modulus of EPS geofoam. These tests were performed on one type of EPS geofoam purchased from a regional producer in the Czech Republic, therefore the results might change slightly if other producers are used. However, the general trend of behavior was in good agreement with previous research. The following conclusions have been reached:

• To evaluate EPS properties from sample tests, a cylindrical shape might have an advantage over the cubic shape due to more uniform pressure distribution on the top and bottom surfaces of the samples.

• A single sample is preferred to a series of samples arranged vertically in layers from top to bottom. Layered configurations tend to collapse due to instability caused by inadequate lateral support of the subsequent samples.

• For a single sample of EPS, as the ratio of height to diameter increases, samples tend to deform in a buckling shape due to lateral instability. In such cases, the ultimate axial strain occurs at a reduced compressive strength depending on the H/D ratio.

• With increasing strain rate, both elastic modulus and compressive strength of the EPS sample increase. The elastic modulus is more sensitive to the strain rate for

denser EPS, while the overall sample strength over the plastic strain region is more sensitive to the strain rate for lighter EPS, which can be attributed to the damage to air bubbles as the applied pressure increases.

• Increasing the EPS sample size (with constant H/D) does not considerably affect the overall stress-strain response of the EPS geofoam. However, the elastic moduli is shown to be dependent on the sample size and this dependency can be expressed in the form of a linear equation.

• The elastic modulus of the EPS samples increases with increasing density of EPS geofoam, and can be related to it using a simple linear function.

• By implementing the stress-strain response from EPS sample tests in a numerical framework, the response of EPS geofoam samples can be reproduced with sufficient accuracy.

• Using the numerical method, EPS samples with D= 300 mm show 47% greater compressive resistance compared to samples with D= 200 mm. The increase in resistance for D= 200 mm compared to D= 100 mm is 21%.

Acknowledgments

Authors of the work presented herein gratefully acknowledge the support in the form of the institutional funding for long-term strategic development of the University of West Bohemia provided by the Ministry of Education of the Czech Republic.

References

Abu-Hejleh, N.M., Zornberg, J.G., Elias, V. and Watcharamonthein, J. (2003), "Design assessment of the founders/meadows GRS abutment structure", *Proceedings of the 82nd Annual Meeting of the Transportation Research Board,* Washington D.C., U.S.A., January.

ASTM D 6817/6817M-17 (2017), Standard Specification for Rigid Cellular Polystyrene Geofoam, American Society for Testing and Materials, West Conshohocken, Pennsylvania, U.S.A.

Azizian, M., Moghaddas Tafreshi, S.N. and Joz Darabi, N. (2020), "Experimental evaluation of an expanded polystyrene (EPS) block-geogrid system to protect buried pipes", *Soil Dyn. Earthq. Eng.*, **129**, 105965. https://doi.org/10.1016/j.soildyn.2019.105965.

Bartlett, S.F., Lingwall, B.N. and Vaslestad, J. (2015), "Methods of protecting buried pipelines and culverts in transportation infrastructure using EPS geofoam", *Geotext. Geomembr.*, **43**(5), 450-461. https://doi.org/10.1016/j.geotexmem.2015.04.019.

Chen, S.J., Yin, D.W., Jiang, N., Wang, F. and Guo, W.J. (2019), "Simulation study on effects of loading rate on uniaxial compression failure of composite rock-coal layer", *Geomech. Eng.*, **17**(4), 333-342. https://doi.org/10.12989/gae.2019.17.4.333.

Chun, B.S., Lim, H.S., Sagong, M. and Kim, K. (2004), "Development of a hyperbolic constitutive model for expanded polystyrene (EPS) geofoam under triaxial compression tests", *Geotext. Geomembr.*, **22**(4), 223-237. https://doi.org/10.1016/j.geotexmem.2004.03.005.

Dehghanbanadaki, A., Motamedi, S. and Ahmad, K. (2020), "FEM-based modelling of stabilized fibrous peat by end-bearing cement deep mixing columns", *Geomech. Eng.*, **20**(1), 75. https://doi.org/10.12989/gae.2020.20.1.075.

Duskov, M. (1991), "Use of expanded polystyrene (EPS) in flexible pavements on poor subgrades", *Proceedings of the International Conference on Geotechnical Engineering for Coastal Development*, Yokohama, Japan, September.

Duškov, M., Houben, L.J.M. and Scarpas, A. (1998), "Response investigation and design guidelines for asphalt pavements with an EPS geofoam sub-base", *Proceedings of the 6th International Conference on Geosynthetics*, Atlanta, Georgia, U.S.A., March.

Elragi, A. (2000), "Selected engineering properties and applications of EPS geofoam", Ph.D. Dissertation, State University of New York, Syracuse, New York, U.S.A.

Elragi, A., Negussey, D. and Kyanka, G. (2001), "Sample size effects on the behavior of EPS geofoam", *Proceedings of the Soft Ground Technology Conference*, Noordwijkerhout, The Netherlands, May-June.

Findley, W.N. and Khosla, G. (1956), "An equation for tension creep of three unfilled thermoplastics", *SPE J.*, **12**(12), 20-25.

Findley, W.N., Lai, J.S. and Onaran, K. (1989), *Creep and Relaxation of Nonlinear Viscoelastic Materials With an Introduction to Linear Viscoelasticity*, Dover Publication, New York, U.S.A.

Frydenlund, T.E. and Aaboe, R. (1994), "Expanded polystyrene-a lighter way across soft ground", *Proceedings of the International Conference on Soil Mechanics and Foundation Engineering*, New Delhi, India, January.

Gao, H, Liu, J. and Liu, H. (2011), "Geotechnical properties of EPS composite soil", *Int. J. Geotech. Eng.*, **5**(1), 69-77. https://doi.org/10.3328/IJGE.2011.05.01.69-77.

Gezgin, A.T. and Cinicioglu, O. (2019), "Consideration of locked-in stresses during backfill preparation", *Geomech. Eng.*, **18**(3), 247-258. https://doi.org/10.12989/gae.2019.18.3.247.

Ghotbi Siabil, S.M.A., Moghaddas Tafreshi, S.N. and Dawson, A.R. (2020), "Response of pavement foundations incorporating both geocells and expanded polystyrene (EPS) geofoam", *Geotext. Geomembr.*, **48**(1), 1-23. https://doi.org/10.1016/j.geotexmem.2019.103499.

Ghotbi Siabil, S.M.A., Moghaddas Tafreshi, S.N., Dawson, A.R. and Parvizi Omran, M. (2019), "Behavior of expanded polystyrene (EPS) blocks under cyclic pavement foundation loading", *Geosynth. Int.*, **26**(1), 1-25. https://doi.org/10.1680/jgein.18.00033.

Hazarika, H. and Okuzono, S. (2004), "Modeling the behavior of a hybrid interactive system involving soil, structure and EPS geofoam", *Soils Found.*, **44**(5), 149-162. https://doi.org/10.3208/sandf.44.5_149.

Hazarika, H. (2006), "Stress-strain modeling of EPS geofoam for large-strain applications", *Geotext. Geomembr.*, **24**(2), 79-90. https://doi.org/10.1016/j.geotexmem.2005.11.003.

Horvath, J.S. (1997), "The compressible inclusion function of EPS geofoam", *Geotext. Geomembr.*, **15**(1-3), 77-120. https://doi.org/10.1016/S0266-1144(97)00008-3.

Horvath, J.S. (1998), "Mathematical modelling of the stress-strain-time behaviour of geosynthetics using the Findley equation: General theory and application to EPS-Block geofoam", CE/GE-98-3, Manhattan College, New York, U.S.A.

Jamshidi Chenari, R., Fatahi, B., Ghorbani, A. and Nasiri Alamoti, M. (2018), "Evaluation of strength properties of cement stabilized sand mixed with EPS beads and fly ash", *Geomech. Eng.*, **14**(6), 533-544. https://doi.org/10.12989/gae.2018.14.6.533.

Jutkofsky, W.S., Teh Sung, J. and Negussey, D. (2000), "Stabilization of embankment slope with geofoam", *Transp. Res. Rec.*, **1736**(1), 94-102. https://doi.org/10.3141/1736-12.

Khalaj, O., Azizian, M., Joz Darabi, N., Moghaddas Tafreshi, S.N.

and Jirková, H. (2020), "The role of expanded polystyrene and geocell in enhancing the behavior of buried HDPE pipes under trench loading using numerical analyses", *Geosciences*, **10**(7), 251. https://doi.org/10.3390/geosciences10070251.

Khalaj, O., M. Azizian, SN Moghaddas Tafreshi, and Mašek, B. (2017), "Laboratory investigation of buried pipes using geogrid and EPS geofoam block", *IOP Conf. Ser. Earth Environ. Sci.*, **95**(2), 022002. https://doi.org/10.1088/1755-1315/95/2/022002.

Khalaj, O., Ghotbi Siabil, S.M.A., Moghaddas Tafreshi, S.N. and Jirkova, H. (2019), "Performance evaluation of pavements constructed on EPS geofoam backfill using repeated plate load test", *IOP Conf. Ser. Earth Environ. Sci.*, **221**(1). https://doi.org/10.1088/1755-1315/221/1/012007.

Kim, B.S., Kato, S. and Park, S.W. (2019), "Experimental approach to estimate strength for compacted geomaterials at low confining pressure", *Geomech. Eng.*, **18**(5), 459-469. https://doi.org/10.12989/gae.2019.18.5.459.

Kwon, Y.M., Chang, I., Lee, M. and Cho, G.C. (2019), "Geotechnical engineering behaviour of biopolymer-treated soft marine soil", *Geomech. Eng.*, **17**(5), 453-464. https://doi.org/10.12989/gae.2019.17.5.453.

Magnan, J.P. and Serratrice, J.F. (1989), "Propriétés mécaniques du polystyrène expansé pour ses applications en remblai routier", *Bull. Liaison Laboratoires Ponts Chaussées*, (164), 25-31.

McDonald, P. and Brown, P.G. (1993), "Ultra lightweight polystyrene for bridge approach fill", *Proceedings of the 11th Southeast Asian Geotechnical Conference*, Singapore, May.

Meguid, M.A. and Hussein, M.G. (2017), "A numerical procedure for the assessment of contact pressures on buried structures overlain by EPS geofoam inclusion", *Int. J. Geosynth. Ground Eng.*, **3**(1), 2. https://doi.org/10.1007/s40891-016-0078-y.

Moghaddas Tafreshi, S.N., Joz Darabi, N., Dawson, A.R. and Azizian, M. (2020), "An experimental evaluation of geocell and EPS geofoam as means of protecting pipes at the bottom of repeatedly loaded trenches", *Int. J. Geomech.*, **20**(4), 04020023. https://doi.org/10.1061/(ASCE)GM.1943-5622.0001624.

Moghaddas Tafreshi, S.N., Joz Darabi, N. and Dawson, A.R. (2020), "Combining EPS geofoam with geocell to reduce buried pipe loads and trench surface rutting", *Geotext. Geomembr.*, **48**(3), 400-418. https://doi.org/10.1016/j.geotexmem.2019.12.011.

Mohajerani, A., Ashdown, M., Abdihashi, L. and Nazem, M. (2017), "Expanded polystyrene geofoam in pavement construction", *Constr. Build. Mater.*, **157**, 438-448. https://doi.org/10.1016/j.conbuildmat.2017.09.113.

Negussey, D., Stuedlein, A., Bartlett, S.F. and Farnsworth, F. (2001), "Performance of a geofoam embankment at 100 south, I-15 reconstruction project, Salt Lake City", *Proceedings of the 3rd International Conference on EPS Geofoam*, Salt Lake City, Utah, U.S.A., December.

Negussey, D. and Sun, M. (1996), "Reducing lateral pressure by geofoam (EPS) substitution", *Proceedings of the International Symposium on EPS Construction Method*, Tokyo, Japan, October.

Negussey, D. and Anasthas, N. (2001), "Young's modulus of EPS geofoam by simple bending test", *Proceedings of the 3rd International Conference on Geofoam Blocks in Construction Applications*, Salt Lake City, Utah, U.S.A., December.

Newman, M.P., Bartlett, S.F. and Lawton, E.C. (2009), "Numerical modelling of geofoam embankments", *J. Geotech. Geoenviron. Eng.*, **136**(2), 290-298. https://doi.org/10.1061/(ASCE)GT.1943-5606.0000203.

Ngo, V.L., Kim, J.M. and Lee, C. (2019), "Influence of structure-soil-structure interaction on foundation behavior for two adjacent structures: Geo-centrifuge experiment", *Geomech. Eng.*, **19**(5), 407-420. https://doi.org/10.12989/gae.2019.19.5.407.

Ossa, A. and Romo, M.P. (2010), "Dynamic characterization of EPS Geofoam", *Geotext. Geomembr.*, **29**(1), 40-50. https://doi.org/10.1016/j.geotexmem.2010.06.007.

Preber, T., Bang, S., Chung, J. and Cho, Y. (1994), "Behaviour of expanded polystyrene blocks", *Transp. Res. Rec.*, **1462**, 36-46.

Selvakumar, S. and Soundara, B. (2019), "Swelling behaviour of expansive soils with recycled geofoam granules column inclusion", *Geotext. Geomembr.*, **47**(1), 1-11. https://doi.org/10.1016/j.geotexmem.2018.08.007.

Sheeley, M. (2000), "Slope stabilization utilizing geofoam", Master's Thesis, Syracuse University, New York, U.S.A.

Simulia, Dassault Systemes. (2013), *ABAQUS 6.13 User's Manual*, Dassault Systems, Providence, RI 305.

Skuggedal, H. and Aaboe, R. (1991), "Temporary overpass bridge founded on expanded polystyrene", *Proceedings of the 1st European Conference on Soil Mechanics and Foundation Engineering*, Florence, Italy.

Srirajan, S. (2001), "Recycled content and creep performance of EPS geofoam in slope stabilization", Master's Thesis, Syracuse University, New York, U.S.A.

Stark, T.D., Arellano, D., Horvath, J.S. and Leshchinsky, D. (2004), "Geofoam applications in the design and construction of highway embankments", NCHRP Web Document 65 (Project 24-11), Transportation Research Board (TRB) of the National Academies.

Tavakoli, H.R., Talebzade Amiri, M., Abdollahzade G. and Janalizade A. (2016), "Site effect microzonation of Babol, Iran", *Geomech. Eng.*, **11**(6), 821-845. https://doi.org/10.12989/gae.2016.11.6.821.

Trandafir, A.C., Bartlett, S.F. and Lingwall, B.N. (2010), "Behavior of EPS geofoam in stress-controlled cyclic uniaxial tests", *Geotext. Geomembr.*, **28**(6), 514-524. https://doi.org/10.1016/j.geotexmem.2010.01.002.

Van Dorp, T. (1996), "Building on EPS geofoam in the "low-lands" experiences in The Netherlands", *Proceedings of the International Symposium on EPS Construction Method*, Tokyo, Japan, October.

Williams, D. and Snowdon, R.A. (1990), "A47 Great Yarmouth western bypass: Performance during the first three years", Contactor Report 211, Transport and Road Research Laboratory.

Wong, H. and Leo, C.J. (2006), "A simple elastoplastic hardening constitutive model for EPS geofoam", *Geotext. Geomembr.*, **24**(5), 299-310. https://doi.org/10.1016/j.geotexmem.2006.03.007.

Zou, Y., Leo, C.J. and Small, J.C. (2000), "Behaviour of EPS geofoam in model test on pavements", *Geosynth. Int.*, **7**(1), 1-22. https://doi.org/10.1680/gein.7.0163.

CC